

Frustrated three-dimensional quantum spin liquid in CuHpCl

M. B. Stone,¹ Y. Chen,¹ J. Rittner,¹ H. Yardimci,¹ D. H. Reich,¹ C. Broholm,^{1,2} D. V. Ferraris,³ and T. LECTKA³

¹*Department of Physics and Astronomy, The Johns Hopkins University, Baltimore, Maryland 21218*

²*National Institute of Standards and Technology, Gaithersburg, Maryland 20899*

³*Department of Chemistry, The Johns Hopkins University, Baltimore, Maryland 21218*

(Received 27 February 2001; revised manuscript received 21 September 2001; published 22 January 2002)

Inelastic neutron scattering measurements are reported for the quantum antiferromagnetic material $\text{Cu}_2(\text{C}_5\text{H}_{12}\text{N}_2)_2\text{Cl}_4$ (CuHpCl). The magnetic excitation spectrum forms a band extending from 0.9 meV to 1.4 meV. The spectrum contains two modes that disperse throughout the **a-c** plane of the monoclinic unit cell with less dispersion along the unique **b**-axis. Simple arguments based on the measured dispersion relations and the crystal structure show that a spin-ladder model is inappropriate for describing CuHpCl. Instead, it is proposed that hydrogen bond mediated exchange interactions between the bi-nuclear molecular units yield a three-dimensional interacting spin system with a recurrent triangular motif similar to the Shastry-Sutherland Model (SSM). Model-independent analysis based on the first moment sum rule shows that at least four distinct spin pairs are strongly correlated and that two of these, including the dimer bond of the corresponding SSM, are magnetically frustrated. These results show that CuHpCl should be classified as a frustration induced three-dimensional quantum spin liquid.

DOI: 10.1103/PhysRevB.65.064423

PACS number(s): 75.10.Jm, 75.40.Gb, 75.50.Ee

I. INTRODUCTION

Organometallic magnets¹ are excellent model systems in which to explore the intricate quantum many-body physics of interacting spin systems.² They are attractive because their energy scales are well matched to efficient experimental probes of magnetism and because a wide range of magnetic phases are found in these materials. In addition to supporting frozen magnetic states with ferromagnetism, ferrimagnetism,³ antiferromagnetism, and metamagnetism, organometallic magnets also provide intriguing examples of quantum spin liquids.^{4,5} These can be defined as strongly correlated states of interacting spin systems where time reversal symmetry persists at temperatures far below the characteristic energy scale for interactions.

Quantum spin liquids are most commonly found in quasi-one-dimensional antiferromagnetic systems such as the uniform spin-1 chain,^{6,7} the alternating spin chain,^{8–12} and the spin-ladder.^{13–16} Low dimensionality generally enhances the phase space for low energy fluctuations,¹⁷ and in one dimension, the effect is to preclude a frozen state involving Heisenberg spins.⁵ However, there are also examples of spin-dimer systems where the singlet ground state associated with antiferromagnetically interacting spin pairs survives the effects of weaker inter-dimer interactions in two and three dimensions.^{18–21}

Geometrical frustration is an alternate route to strong fluctuations,^{5,22} and there are theoretical predictions²³ of quantum^{24,25} and classical²⁶ spin liquids based on this effect. While materials that approximate kagome^{27,28} and pyrochlore^{29,30} antiferromagnets generally have a freezing transition at sufficiently low temperatures, there are other more complex structures where geometrical frustration stabilizes an isolated singlet ground state in the $T=0$ limit.^{31–33} $\text{SrCu}_2(\text{BO}_3)_2$ is a three-dimensional version of the so-called Shastry-Sutherland model³⁴ where the interdimer interactions are almost as strong as the intra-dimer interactions, and

yet they fail to induce gapless magnetic fluctuations and long range order because no such state can satisfy all interactions.^{32,35} Frustration is also central to stabilizing the quasi-two-dimensional cooperative singlet state in the organometallic magnet PHCC.³³ While in $\text{SrCu}_2(\text{BO}_3)_2$ correlations exist only within spin-dimers,³⁵ the correlated spin clusters in PHCC involve at least eight spins of which two spin pairs are frustrated and provide a positive contribution to the ground state energy. PHCC was previously identified as an alternating spin chain based on susceptibility measurements. This and other misidentifications^{11,12} indicate that conventional bulk measurements cannot reliably determine the origin and nature of spin systems with a gapped excitation spectrum and that more sophisticated techniques should be applied to explore these unique systems.

One magnet with a gapped excitation spectrum that has received considerable attention is $\text{Cu}_2(\text{C}_5\text{H}_{12}\text{N}_2)_2\text{Cl}_4$ [$\text{Cu}_2(1,4\text{-diazacycloheptane})_2\text{Cl}_4$, or for short CuHpCl].^{36–49} Measurements of the magnetization, magnetic susceptibility, and specific heat show that this system has a spin gap $\Delta \approx 0.9$ meV, a magnetic bandwidth of approximately 0.5 meV, and a saturation field $H_{c2} = 13.2$ T. Based on these measurements and the crystal structure, it was proposed that CuHpCl is a two-leg spin ladder composed of coupled dimers, with the intra-dimer bonds of strength $J_1 = 1.14$ meV forming the rungs, and inter-dimer bonds of strength $J_2 \approx 0.2J_1$ forming the legs of the ladders.³⁸ Subsequent experimental results have generally been interpreted in terms of this model, and the system has been the inspiration for a number of theoretical studies.^{50–58}

Despite this extensive body of work, the true nature of the spin interactions in CuHpCl has never been conclusively demonstrated. Susceptibility and specific heat data are equally well described by spin-ladder, alternating chain, and coupled-bilayer models.⁵⁰ Some evidence that the two-leg ladder model might in fact not be appropriate for CuHpCl came from a previous inelastic neutron scattering

experiment⁴¹ on a powder sample, where we found that the wave vector-integrated magnetic scattering intensity did not show the characteristic van Hove singularities expected for the magnetic density of states of a one-dimensional spin system. In this measurement, the wave vector dependence of the energy-integrated magnetic scattering was also inconsistent with the predictions of the ladder model. However, conclusions from this experiment were limited by the coarse wave vector resolution of the instrument employed, and the large, nonmagnetic background signal from the hydrogenous sample.

In this paper, we report inelastic neutron scattering measurements performed both on a deuterated powder with improved wave vector resolution and on hydrogenous single crystals. The powder and single-crystal measurements are each independently inconsistent with the spin-ladder model. The powder data indicate that the strongest dimer bond is different from that of the ladder model. The single-crystal measurements show the presence of two modes within the 0.5 meV bandwidth, a feature not predicted by the spin-ladder model. Consideration of the measured dispersion relation and the structure of the system lead to the conclusion that the network of significant magnetic interactions in CuHpCl is three dimensional. Model-independent analysis of the powder and single-crystal data based on the first moment sum rule provide the contributions of each crystallographically distinct spin pair to the ground state energy. Two classes of spin pairs yield positive contributions, indicating that geometrical frustration plays an important role in stabilizing the quantum spin liquid in CuHpCl.

Structure of CuHpCl

CuHpCl is monoclinic with space group $P2_1/c$ and room temperature lattice constants $a = 13.406(3)$ Å, $b = 11.454(2)$ Å, $c = 12.605(3)$ Å, and $\beta = 115.01(2)^\circ$.³⁶ The low-temperature lattice constants measured with neutron scattering at $T = 4$ K are $a = 13.35(4)$ Å, $b = 11.24(6)$ Å, $c = 12.72(4)$ Å, and $\beta = 115.2(2)^\circ$. Figure 1 shows the approximately centro-symmetric binuclear molecular unit containing the spin pair denoted by bond 1 in Table I. Each Cu^{2+} ion is in a (4+1) square pyramidal coordination with a Cl atom at the apex and the base formed by two N and two Cl atoms. Within the $\text{Cu}(\mu\text{-Cl})_2\text{Cu}$ complex of CuHpCl, the coordinating pyramids share apical edges and have parallel basal planes. Susceptibility measurements for a series of compounds with this atomic configuration indicate intramolecular exchange constants ranging from -1.5 meV (ferromagnetic) to 0.9 meV (AFM) with no apparent correlation throughout the range of molecular structural parameters.⁵⁹

The intramolecular exchange interactions in CuHpCl do not create an extended lattice. Because the molecular units in CuHpCl interact solely through hydrogen bonding, the dimensionality and the overall nature of magnetic interactions in this system are entirely determined by hydrogen bond mediated exchange interactions. Owing to the slight deviation of the CuHpCl molecules from centro-symmetry, molecular pairs come in two flavors in the CuHpCl crystal structure,

TABLE I. Cu-Cu bond lengths and fractional coordinates for CuHpCl calculated from previously determined atomic coordinates (Ref. 36) and measured low temperature ($T = 4$ K) lattice constants. The lattices of interacting spins formed by the bonds are shown in Fig. 3 and Fig. 14. The last column shows the contribution of each spin pair to the ground state energy. Bonds with the same numerical index are closely related in terms of bond vectors and chemical environments such that their contributions cannot and need not be distinguished in this experiment.

Bond ID	d (Å)	x/a	$\pm y/b$	z/c	$J_{\mathbf{a}}\langle\mathbf{S}_0 \cdot \mathbf{S}_{\mathbf{a}}\rangle$ (meV)
1	3.376	0.179	0.231	0.089	0.42(3)
2a	5.757	0.331	0.234	0.399	0.06(4)
2b	5.813	0.312	0.227	0.423	
3a	6.987	0.509	0.003	0.488	-0.29(3)
3b	7.000	0.491	0.003	0.512	
4a	7.024	0	0.266	0.5	-0.18(1)
4b	7.057	0	0.273	0.5	
5a	7.154	0.491	0.269	0.012	0.06(2)
5b	7.502	0.509	0.269	-0.012	
6a	7.303	0.312	0.5	-0.077	-0.05(4)
6b	7.586	0.331	0.5	-0.101	
7a	8.648	0.179	0.497	-0.411	-0.09(7)
7b	8.698	0.179	0.503	-0.411	
8a	8.814	0.179	0.497	0.589	-0.15(3)
8b	8.863	0.179	0.503	0.589	
9	8.910	0.179	0.769	0.089	0.1(2)
10a	9.327	0.669	0.234	0.601	0.01(6)
10b	9.343	0.688	0.227	0.577	

which we denote by a and b . Neglecting flavor distinctions, there are four configurations for molecular pairs in direct contact, as shown in Fig. 2. The sublattices generated by each of these pairs are shown in Fig. 3. The numbers on Fig. 3 indicate possible spin exchange interactions mediated by hydrogen bonding, and additional information about each of these is listed in Table I. Each molecule is part of two molecular pairs of the type shown in Fig. 2(a). The three different exchange interactions associated with this molecular pair are denoted 2, 3, and 10 in Fig. 3 and Table I. Bonds 2 and 3 proceed through a Cu-N-H-Cl-Cu path with H-Cl distances ranging from 2.3 Å to 2.7 Å. Bond 10 has a similar exchange pathway as for bonds 2 and 3 but must in addition traverse the entire $\text{Cu}(\mu\text{-Cl})_2\text{Cu}$ complex. The corresponding exchange interaction should therefore be significantly weaker than for bonds 2 and 3. Each molecule is also part of four pairs of the type shown in Fig. 2(b). Exchange pathways involving Cu-N-C-H-Cl-Cu mediate two different exchange interactions that we denote 4 and 7, with H-Cl bond distances ranging from 2.6 Å to 2.8 Å. Bond 7 should be negligible, however, as it involves an apical Cu-Cl contact. The same molecular pairs also afford an exchange interaction denoted by 8, which proceeds through a Cu-Cl-H-C-H-Cl-Cu pathway with H-Cl bond distances in the range 2.6 – 3.0 Å. Each molecule also is part of four molecular pairs of the type shown in Fig. 2(c). The exchange pathway involves either Cu-Cl-H-C-N-Cu or Cu-N-H-H-C-N-Cu with H-Cl and H-H bond lengths ranging from 2.7 Å to 3.1 Å. The correspond-

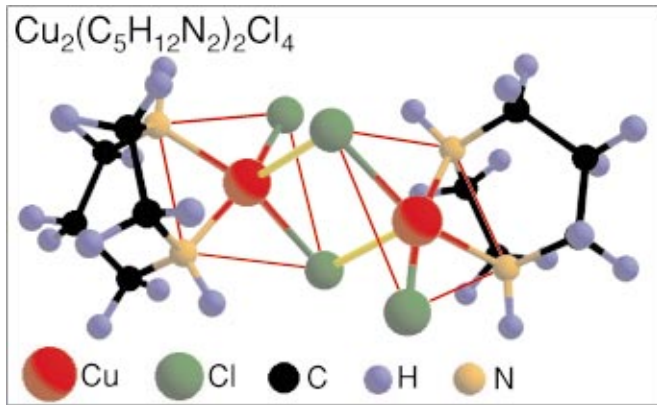


FIG. 1. (Color) The molecular formula unit of CuHpCl featuring two copper atoms in 4+1 square pyramidal coordination (Ref. 36). The apical Cu-Cl bonds are shown in yellow. The Cu coordination pyramids share an apical edge and have parallel basal planes (red lines).

ing exchange interactions are denoted 5 and 6. Finally, each molecule is also part of two molecular pairs of the type shown in Fig. 2(d) with displacement vectors $\pm \mathbf{b}$. The exchange path passes through two 1,4-diazacycloheptane rings so the corresponding interactions are likely to be negligible, especially considering the lower coordination number for this interaction.

The molecular pairs in Figs. 2(a) and 2(d) yield one-dimensional lattices extending along the $[101]$ and $[010]$ directions, respectively. Intermolecular interactions corresponding to Figs. 2(b) and 2(c), on the other hand, yield $\mathbf{b}\text{-c}$ and $\mathbf{a}\text{-b}$ spin planes with surface normals \mathbf{a}^* and \mathbf{c}^* , respectively. Unfortunately it is difficult to predict the strength of hydrogen mediated exchange interactions, which reportedly can range from 0.1 meV to greater than 10 meV depending on the chemical environment.⁶⁰ Previous papers on CuHpCl worked under the assumption that the intermolecular bonds depicted in Fig. 2(a) are dominant, leading to the ladder model shown in Fig. 3(a). While we cannot provide firm quantitative information about the magnitude of intermolecular exchange interactions, we shall present evidence that the eight intermolecular pairs of the type shown in Figs. 2(b)–2(c) when combined are energetically more significant than those shown in Fig. 2(a), and that the intra-molecular spin pair (1) is in a frustrated configuration.

II. EXPERIMENTAL TECHNIQUES

The powder sample studied consisted of 5.87 grams of deuterated CuHpCl. To produce this sample, perdeuterated 1,4-diazacycloheptane was first prepared following a previously published method.⁶¹ The d_6 -dibromopropane and N,N' -dibenzylethylene- d_4 -diamine precursors required for this synthesis were prepared from commercially available 1,3- d_6 -propanediol and ethylene- d_4 -diamine, respectively. The CuHpCl powder was obtained by rapid cooling from 40 °C to 0 °C of 1:1 molar solutions of anhydrous CuCl_2 and the deuterated 1,4-diazacycloheptane dissolved in the minimum amount of deuterated methanol. Prompt gamma neu-

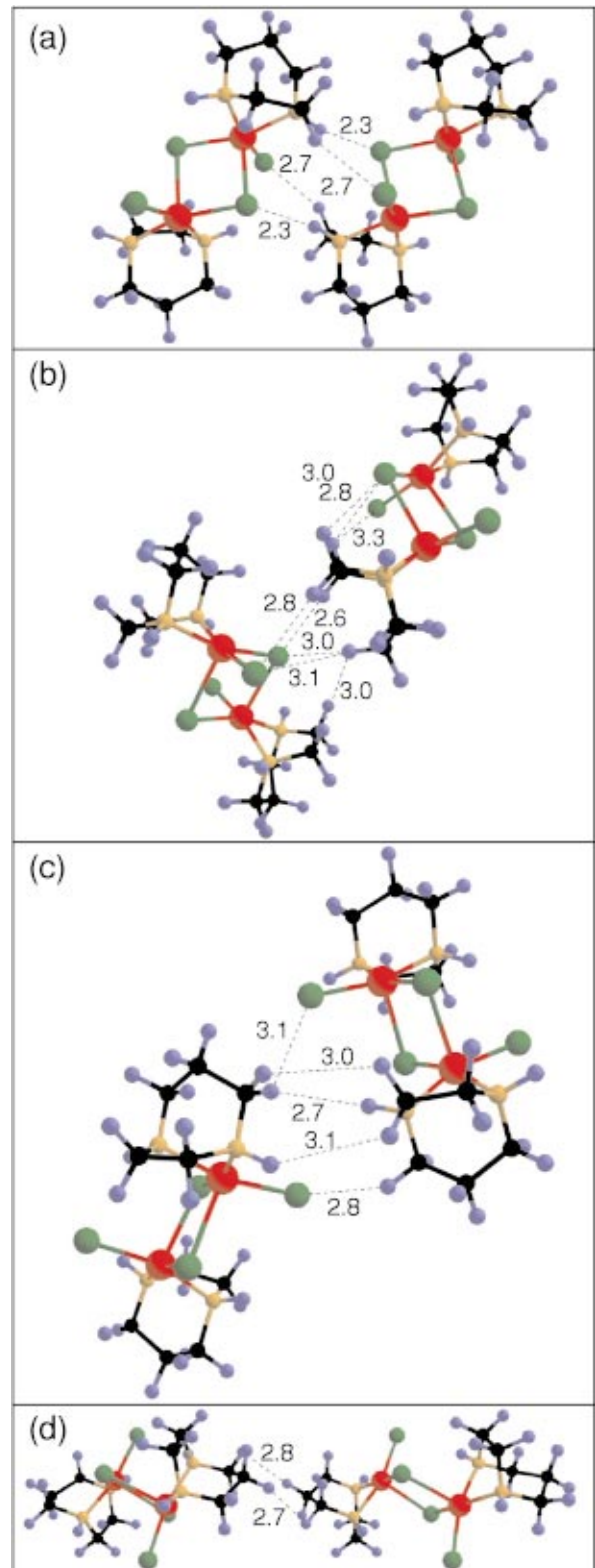


FIG. 2. (Color) The four different types of near neighbor hydrogen bonded molecular pairs in CuHpCl (Ref. 36). Numbers indicate hydrogen bond distances in Å. The orientations of the molecules correspond to the lattices of interactions shown in Fig. 3. Color coding is the same as for Fig. 1.

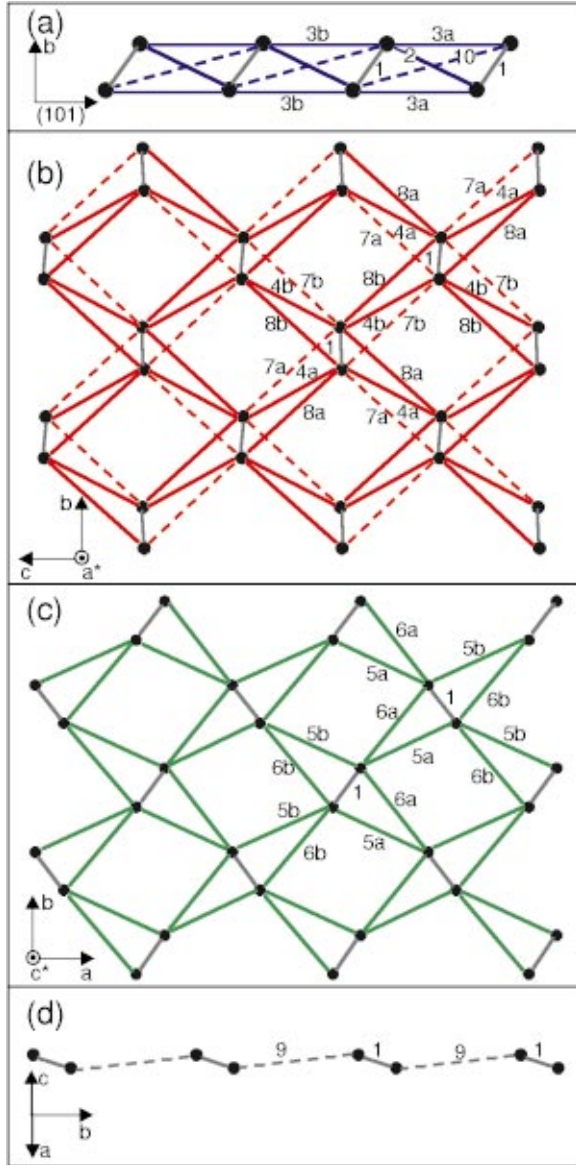


FIG. 3. (Color) The four different types of lattices generated by the intermolecular interactions shown of Figs. 2(a)–2(d). The molecules in Figs. 2 are oriented like the spin pairs indicated by 1 in this figure. Dashed lines indicate interactions that are expected to be very weak. Bond numbers refer to Table I. Sublattice color coding coincides with that of Fig. 14.

tron activation analysis performed on a portion of the sample confirmed 95.0(1)% deuteration.

The single-crystal measurements were performed on a composite sample with a total mass $m \approx 110$ mg. This sample consisted of four hydrogenous single crystals, mutually aligned to within 4.5 deg. These crystals were obtained by diffusive growth from CuCl_2 and 1,4-diazacycloheptane in methanol.⁴⁷ We have produced crystals as large as 33 mg using this method.

Inelastic neutron scattering measurements on both the powder and single-crystal samples were performed using the SPINS cold neutron triple axis spectrometer at the National Institute of Standards and Technology in Gaithersburg,

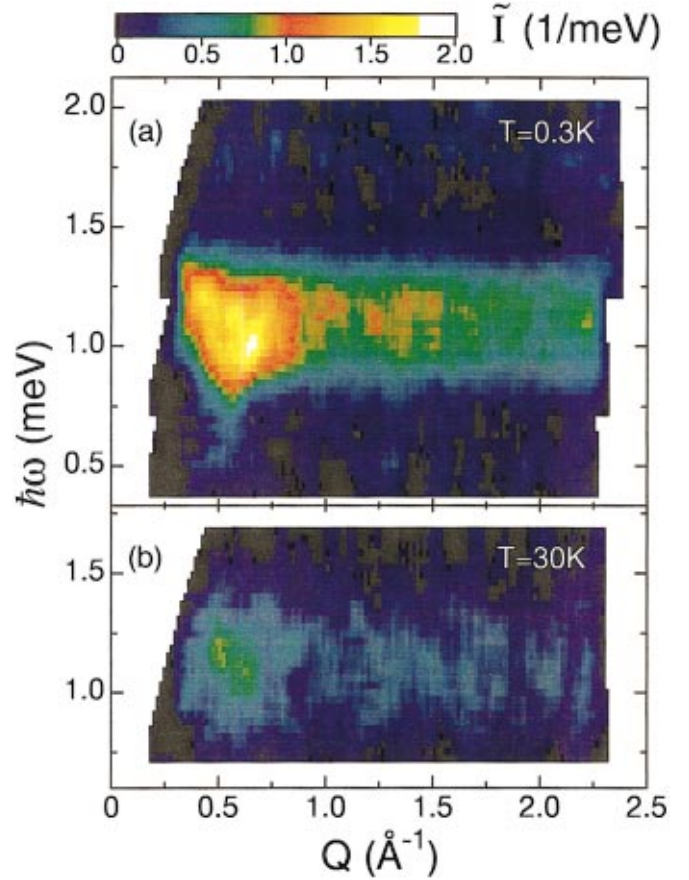


FIG. 4. (Color) Powder inelastic neutron scattering intensity $\tilde{I}(Q, \hbar\omega)$ for CuHpCl at (a) $T=0.3$ K, and (b) $T=30$ K obtained by combining measurements at $E_i=4.84, 4.3,$ and 4.0 meV. The figure was produced by binning the data in bins of size $\delta\hbar\omega=0.03$ meV and $\delta Q=0.016$ \AA^{-1} and then coarse-grain averaging to set the effective resolution to $\Delta\hbar\omega=0.2$ meV and $\delta Q=0.08$ \AA^{-1} .

Maryland. For the powder experiment, the horizontal beam collimation before the sample was $50'/k_i$ (\AA^{-1})- $80'$. Scattered neutrons in the energy range $2.6 \text{ meV} \leq E_f \leq 3.7$ meV were Bragg reflected by a flat, 23 cm wide by 15 cm high pyrolytic graphite analyzer [PG(002)] at a distance of 91 cm from the sample position. The analyzer was followed by an $80'$ radial collimator and a position-sensitive detector. Cooled Be and BeO filters were employed before and after the sample, respectively. Data were collected by scanning the scattering angle 2θ in the range 7° to 114° at fixed incident energy E_i . Scans at $E_i=4.0, 4.34,$ and 4.84 probed inelastic scattering for energy transfer $0.4 \text{ meV} \leq \hbar\omega \leq 2.09$ meV and momentum transfer $0.2 \text{ \AA}^{-1} \leq Q \leq 2.35 \text{ \AA}^{-1}$, with average full width at half maximum (FWHM) resolutions $\delta\hbar\omega=0.14$ meV and $\delta Q=0.014 \text{ \AA}^{-1}$.⁶² Backgrounds due to incoherent scattering from the analyzer and low-angle air scattering of the incident neutron beam were measured separately. After subtracting these, the data were converted to the normalized scattering intensity $\tilde{I}(Q, \hbar\omega)$ using the measured incoherent elastic scattering from the sample following the procedure detailed in Ref. 41.

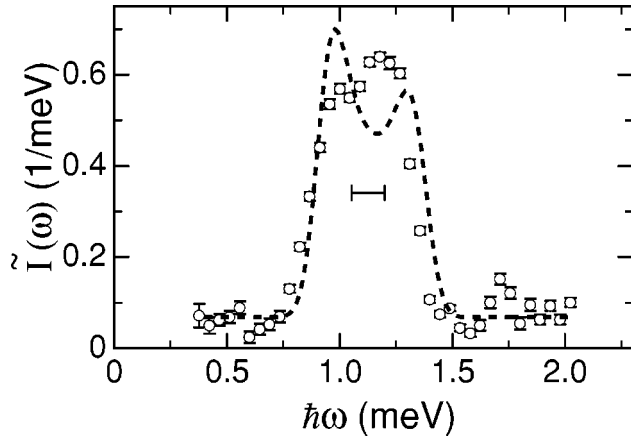


FIG. 5. Wave vector-averaged scattering intensity vs energy transfer for CuHpCl. The region of integration is limited to $0.3 \text{ \AA}^{-1} < Q < 2.3 \text{ \AA}^{-1}$. The horizontal bar indicates the FWHM energy resolution. The dashed line shows the resolution convoluted spectrum for the previously accepted spin-ladder model (Ref. 41).

For the single-crystal measurements, the horizontal beam collimation before the sample was $50' / k_i (\text{\AA}^{-1}) - 80'$. A liquid nitrogen cooled BeO filter was placed after the sample and data were collected at fixed final energy $E_f = 3.7 \text{ meV}$ while scanning the incident energy in the range $3.95 \leq E_i \leq 5.45 \text{ meV}$. A horizontally focusing pyrolytic graphite analyzer with horizontal and vertical acceptance angles of 5° and 7° , respectively, was used in conjunction with a single cylindrical detector, which subtended an angle of 4° in the horizontal plane to an area element of the analyzer. In this configuration the average instrumental energy resolution for the energy transfer range of $0.75 - 1.25 \text{ meV}$ was $\delta \hbar \omega \approx 0.17(1) \text{ meV}$. Representative values of the projected FWHM wave vector resolution for the constant- Q scans performed throughout the measurement are $\delta Q_{\parallel} = 0.081 \text{ \AA}^{-1}$ and $\delta Q_{\perp} = 0.065 \text{ \AA}^{-1}$ for the components of the wave vector transfer along the principal directions of the resolution ellipse at $\mathbf{Q} = (100)$ and $\hbar \omega = 1 \text{ meV}$. Scans at constant wave vector transfer were performed in both the $(h0l)$ and $(hk0)$ reciprocal lattice planes.

III. RESULTS

A. Powder sample measurements

Figure 4 shows the normalized scattering intensity $\tilde{I}(Q, \hbar \omega)$ for CuHpCl at $T = 0.3 \text{ K}$ and $T = 30 \text{ K}$. At $T = 0.3 \text{ K}$, there is a band of inelastic scattering in the range of energy transfer $0.9 \text{ meV} < \hbar \omega < 1.4 \text{ meV}$, consistent with our previous measurements on a hydrogenous powder sample.⁴¹ At $T = 30 \text{ K}$, the intensity in this $Q - \hbar \omega$ range is diminished, which confirms that the corresponding inelastic scattering cross section is magnetic.

Figure 5 shows the wave vector averaged scattering intensity

$$\tilde{I}(\omega) = \frac{\int Q^2 dQ \tilde{I}(Q, \omega)}{\int Q^2 dQ}. \quad (1)$$

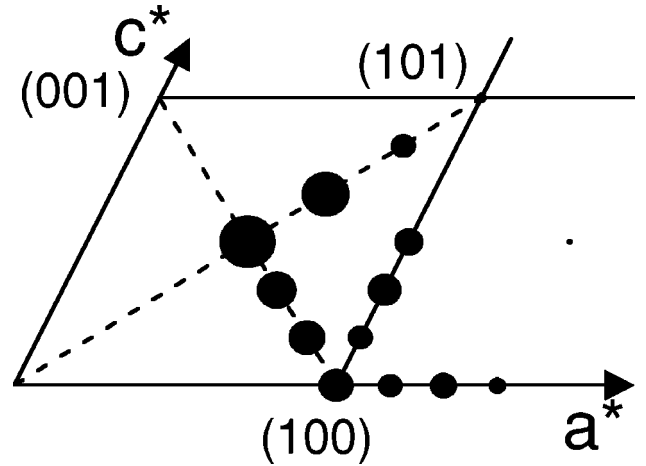


FIG. 6. Locations in the $(h0l)$ plane at which single-crystal inelastic neutron scattering data was obtained for CuHpCl. The diameters of the points are proportional to the measured first moment of the data, and show that the dominant satisfied magnetic bond is parallel to $[101]$.

These data are a measure of the magnetic density of states. One-dimensional magnets have pronounced van Hove singularities at the upper and lower bounds of the magnetic excitation spectrum. When convolved with the energy resolution function, such singularities would produce the spectrum shown by the dashed line in Fig. 5.⁴¹ The inconsistency between model and data provides a first indication that CuHpCl is not a one-dimensional spin system. A previous experiment led to the same conclusion,⁴¹ and as it was done on a hydrogenous sample while the present sample is deuterated, the comparison of these experiments indicates that deuteration does not significantly alter magnetism in CuHpCl. Figure 4(a) also shows that inelastic magnetic neutron scattering from CuHpCl is strongly peaked near $Q_0 \approx 0.6 \text{ \AA}^{-1}$, with a secondary maximum near 1.3 \AA^{-1} . The powder averaged scattering intensity from a single spin dimer with spacing d has a peak for $Q_0 d = 1.43\pi$.⁶³ The data thus indicate singlet formation in CuHpCl between spins separated by $d \approx 1.43\pi / Q_0 = 7.5 \text{ \AA}$. This result is also inconsistent with the ladder model for CuHpCl, as the dominant bond in this model is the intramolecular Cu pair (Fig. 1) whose spacing is only $d_1 = 3.376 \text{ \AA}$.

B. Single-crystal measurements

Inelastic scattering measurements were carried out at $T = 1.4 \text{ K}$ for wave vector transfers at the locations in the $(h0l)$ plane indicated on Fig. 6, as well as along the line $(1k0)$ perpendicular to this plane. Figures 7–11 show the data so obtained, while Figs. 12 and 13 summarize the corresponding dispersion relations derived by fitting the constant wave vector scans to resolution limited peaks.

When dynamic correlations are dominated by a single dimerized spin pair, there is a well tested RPA theory that can account for many aspects of the magnetic excitation spectrum.^{18–21} As we shall show in the following, each spin in CuHpCl takes part in several strongly correlated spin

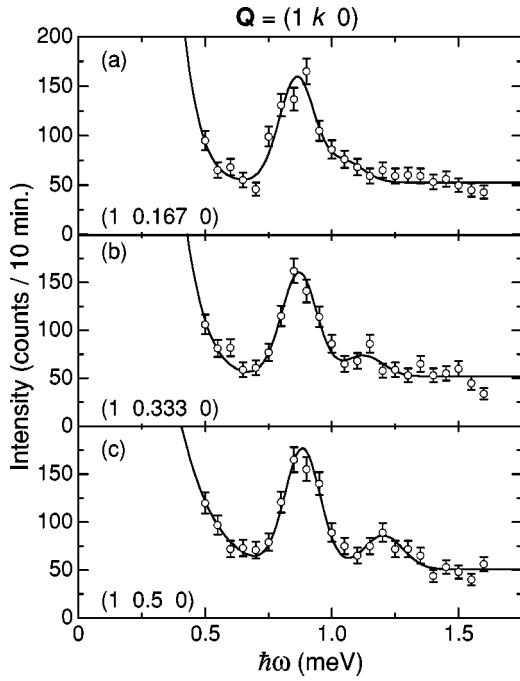


FIG. 7. Inelastic neutron scattering data for CuHpCl at $T = 1.4$ K indicating less than 0.05 meV dispersion along the $(1k0)$ direction. The scan at $(1,0.5,0)$ shows the presence of two modes in the excitation spectrum. Solid lines are fits to resolution limited Gaussians.

pairs, so the RPA theory is not applicable in its present form. However, inspection of the excitation spectra and the crystal structure leads to important insights concerning the magnetism in CuHpCl.

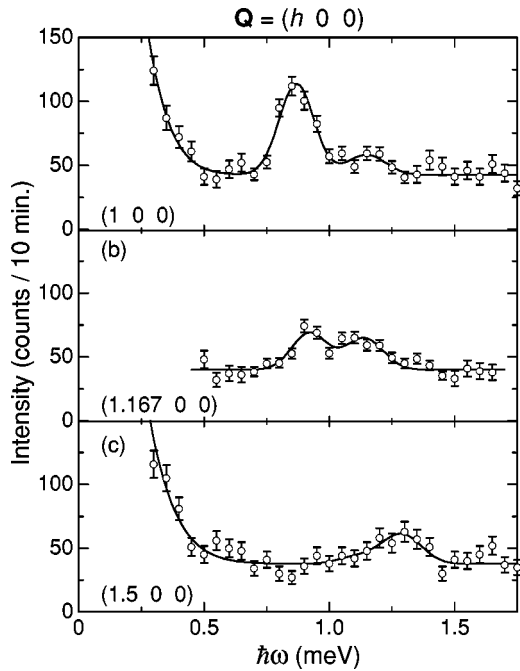


FIG. 8. Inelastic neutron scattering data for CuHpCl at $T = 1.4$ K showing dispersion along $(h00)$, which is perpendicular to the lattice in Fig. 3(b). Solid lines are fits to resolution limited Gaussians.

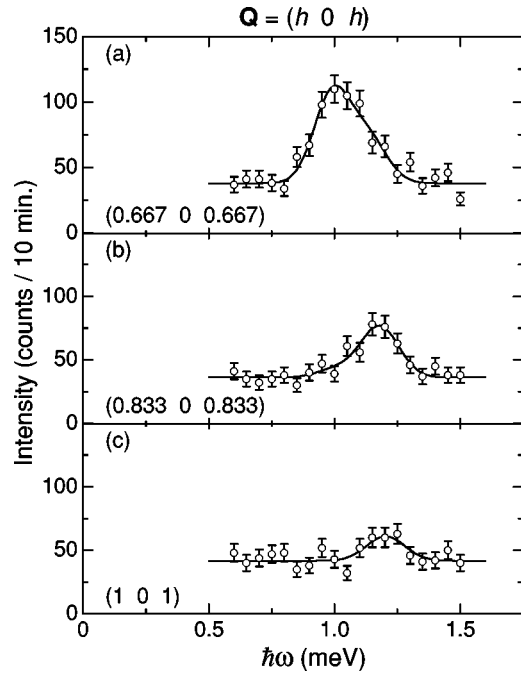


FIG. 9. Inelastic neutron scattering data for CuHpCl at $T = 1.4$ K indicating dispersion along the $(h0h)$ direction. Solid lines are fits to resolution limited Gaussians.

We first note that there are two modes in the magnetic excitation spectrum. This is most easily seen at $\mathbf{Q} = (1,0.5,0)$ in Fig. 7(c), where two resolution-limited peaks are clearly visible at $\hbar\omega = 0.88$ and 1.2 meV. Two modes are also visible at other wave vectors such as $\mathbf{Q} = (1.167,0,0)$ in

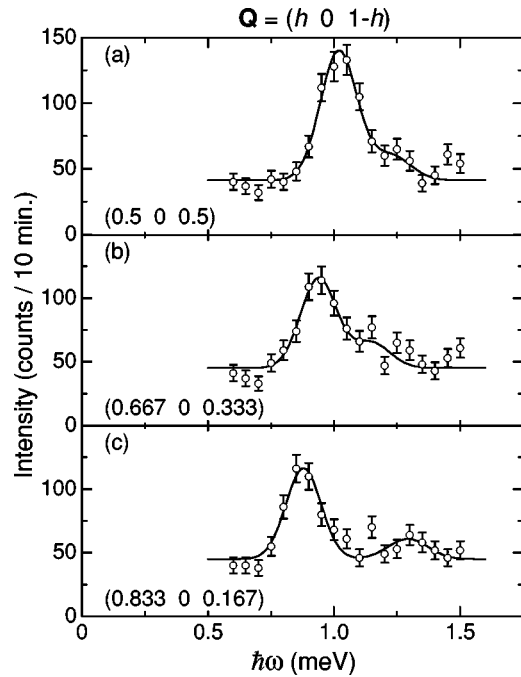


FIG. 10. Inelastic neutron scattering data for CuHpCl at $T = 1.4$ K showing dispersion along the $(h,0,1-h)$ direction, which is perpendicular to the spin ladder in Fig. 3(a). Solid lines are fits to resolution limited Gaussians.

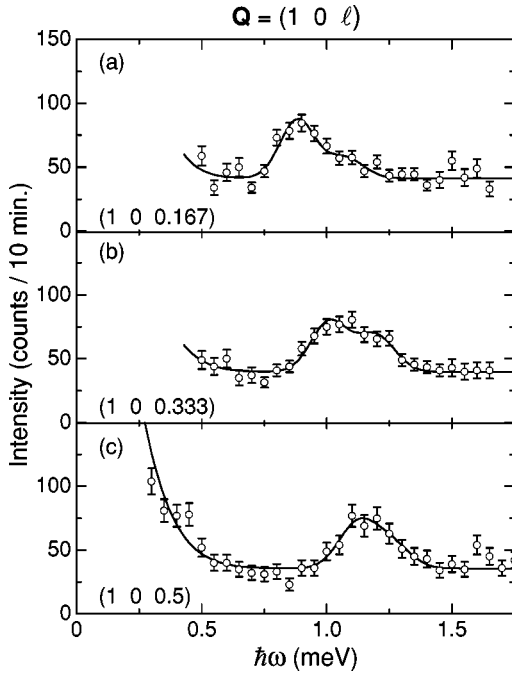


FIG. 11. Inelastic neutron scattering data for CuHpCl at $T = 1.4$ K. (a)–(c) show dispersion along the $(10l)$ direction which is perpendicular to the lattice in Fig. 3(c). Solid lines are fits to resolution limited Gaussians.

Fig. 8(b). In addition, Fig. 9(a) and Figs. 11(a)–11(c) show broad or asymmetric peaks that are well described by a superposition of two resolution-limited Gaussian peaks.

The spin-ladder and alternating chain models for CuHpCl corresponding to Figs. 3(a) and 3(d), respectively, both have

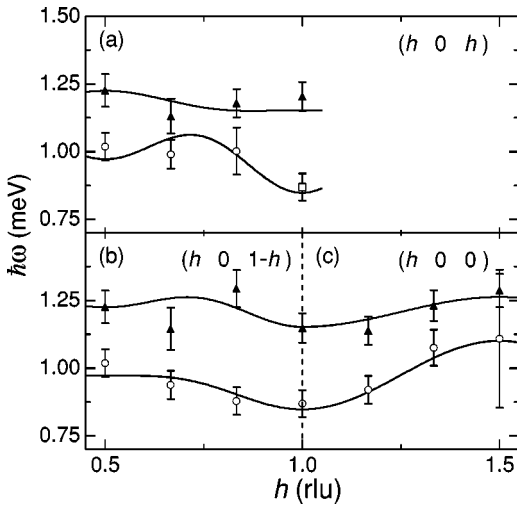


FIG. 12. Dispersion of magnetic excitations in CuHpCl derived from the fits shown in Figs. 8, 9, and 10. Open circles represent the lower energy mode, solid triangles represent the higher energy mode. Solid lines are phenomenological fits to a dispersion relation satisfying Bloch's theorem: $\hbar\omega(\mathbf{Q}) = A_0 + A_1 \cos 2\pi h + A_2 \cos 2\pi l + A_3 \cos 2\pi(h+l) + A_4 \cos 2\pi(h-l)$. Assuming no mode crossing, the constants are 1.00(2) meV, $-0.04(2)$ meV, $-0.02(2)$ meV, $-0.07(2)$ meV, and $-0.02(2)$ meV for the lower mode and 1.21(2) meV, $-0.03(2)$ meV, 0.00(2) meV, 0.01(2) meV, and $-0.03(2)$ meV for the upper mode respectively.

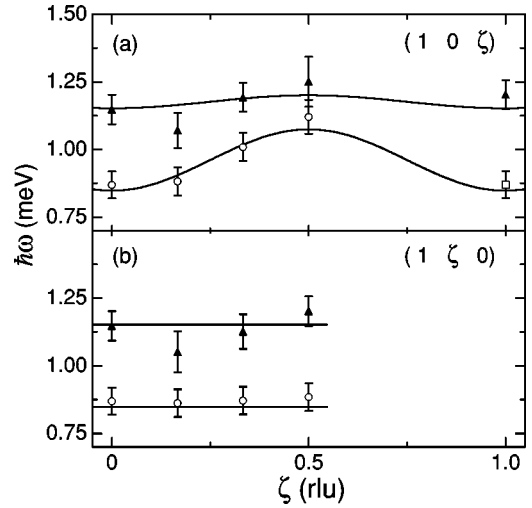


FIG. 13. Dispersion of magnetic excitations in CuHpCl derived from the data shown in Figs. 7 and 11. Open circles represent the lower energy mode, solid triangles represent the higher energy mode, and the open square point at (101) represents the energy of the dominant mode at (100) translated by $\tau = (001)$. Solid lines are phenomenological fits as described in the caption to Fig 12.

a single degenerate triplet excitation and are therefore inconsistent with the observed two modes. This is true despite the fact that $\text{Cu}(\mu\text{-Cl})_2\text{Cu}$ complexes in CuHpCl come with two different orientations as the intermolecular interactions in Figs. 2(a) and 2(d) only couple molecules with like orientations. However, the intermolecular interactions in Figs. 2(b) and 2(c) link molecules with different orientations to form lattices with two molecules per unit cell [Figs. 3(b) and 3(c)]. If the ground and excited states maintain the full symmetry of the paramagnetic molecule and the spectrum is dominated by resonant modes, then any lattice except those in Figs. 3(a) and 3(d) has two triplet excited states consistent with the experimental data. This means that the lattices shown in Fig. 3(b) and/or 3(c) are essential parts of the interacting spin system in CuHpCl.

This conclusion is reinforced by Figs. 10 and 12(b), which show dispersion along the $(h01-h)$ direction [equivalent to $(h0\bar{h})$]. With displacement vectors along $[101]$ and $[010]$, the molecular pairs in Figs. 2(a) and 2(d) cannot yield dispersion along this direction in reciprocal space. The implication is again that the intermolecular interactions shown in Figs. 2(b) and/or 2(c), and hence the lattices shown in Figs. 3(b) and/or 3(c), are essential parts of the cooperative magnetic network in CuHpCl. Figures 8 and 12(c) show that there is also dispersion along the \mathbf{a}^* direction. This implies that the interactions corresponding to Figs. 2(b) and 3(b) cannot be the only relevant intermolecular interactions in the problem. Figures 11 and 13(a) show that there is dispersion along the \mathbf{c}^* direction. Consequently the interactions corresponding to Figs. 2(c) and 3(c) also cannot be the only relevant intermolecular interactions. By inference, at least two of the four types of intermolecular interactions in Fig. 2 are important to cooperative magnetism in CuHpCl, and the interactions in Figs. 2(b) and/or 2(c) must be part of the group.

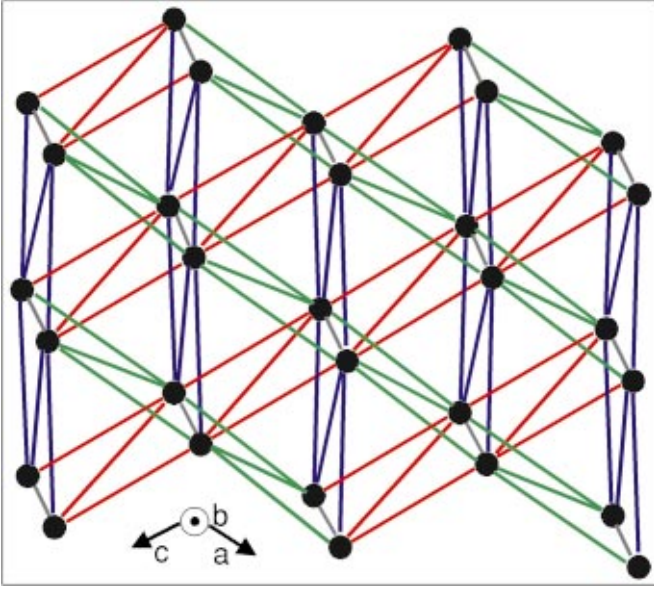


FIG. 14. (Color) The combined lattice of spin-spin interactions in CuHpCl viewed as a projection on the **a-c** plane with the same color coding as for the individual sublattices in Fig. 3.

Figure 14 shows a projection of the lattice of interactions in CuHpCl along the **b** direction. The color-coding is consistent with Fig. 3 indicating bonds associated with different intermolecular interactions. As the lattices of Fig. 3 interpenetrate, a corollary to the above is that CuHpCl is a three-dimensional interacting spin system. Nonetheless, Figs. 7 and 13 show that there is less than 0.05 meV dispersion along $\mathbf{Q}=(1k0)$. Based on the discussion above, the absence of dispersion along **b** cannot be due to lack of interactions that couple the system magnetically. A likely alternate explanation is that geometrical frustration localizes the excitations as has been observed in other geometrically frustrated systems.^{29,35,64}

IV. ANALYSIS

Wave vector dependent intensity

The dynamic spin correlation function $S(\mathbf{Q},\omega)$ obeys sum-rules that can be used to draw additional model independent conclusions about magnetism in CuHpCl. The total moment sum-rule⁶⁵ provides an important check on whether the measured scattering intensity accounts for all spins in the sample:

$$\frac{\int d^3\mathbf{Q} \int \hbar d\omega \sum_{\alpha} S^{\alpha,\alpha}(\mathbf{Q},\omega)}{\int d^3\mathbf{Q}} = S(S+1). \quad (2)$$

The first moment sum-rule⁶⁶ provides a direct link between raw data and interaction terms in the spin Hamiltonian:

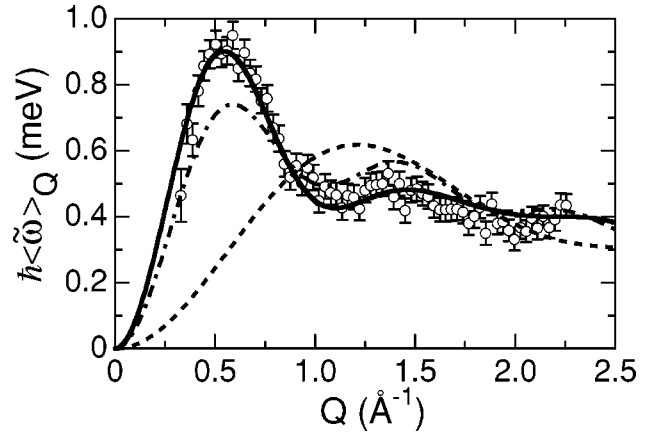


FIG. 15. First $\hbar\omega$ moment of the inelastic powder data in Fig. 4 versus wave vector transfer [Eq. (7)]. The region of integration is limited to the band of magnetic excitations from 0.7 to 1.5 meV. The dashed-dotted line is a fit with a single dimer bond length of 7.5(2) Å. The dashed line is a fit fixing the dimer bond length to 3.376 Å, corresponding to the intra molecular Cu-spacing. The solid line is the best combined fit to the powder and single crystal data. Fit results are described in the text and enumerated in Table I

$$\hbar\langle\omega\rangle_{\mathbf{Q}} \equiv \hbar^2 \int_{-\infty}^{\infty} \omega S^{\alpha\alpha}(\mathbf{Q},\omega) d\omega \quad (3)$$

$$= -\frac{1}{3} \frac{1}{N} \sum_{\mathbf{r},\mathbf{d}} J_{\mathbf{d}} \langle \mathbf{S}_{\mathbf{r}} \cdot \mathbf{S}_{\mathbf{r}+\mathbf{d}} \rangle (1 - \cos \mathbf{Q} \cdot \mathbf{d}). \quad (4)$$

Here $\{\mathbf{d}\}$ is the set of all bond vectors connecting a spin to its neighbors, the index $\{\mathbf{r}\}$ runs over all N spins. The Hamiltonian is assumed to take the form

$$\mathcal{H} = \frac{1}{2} \sum_{\mathbf{r},\mathbf{d}} J_{\mathbf{d}} \mathbf{S}_{\mathbf{r}} \cdot \mathbf{S}_{\mathbf{r}+\mathbf{d}}, \quad (5)$$

For a powder sample, the magnetic component of $\tilde{I}(Q,\hbar\omega)$ is related to the spherically averaged dynamic spin correlation function $S(Q,\omega)$ by⁴¹

$$\tilde{I}_m(Q,\hbar\omega) = 2 \int dQ' \hbar d\omega' \mathcal{R}_{Q\omega}(Q-Q',\omega-\omega') \times \left| \frac{g}{2} f(Q') \right|^2 S(Q',\omega'), \quad (6)$$

where $\mathcal{R}_{Q\omega}(\delta Q, \delta\omega)$ is the normalized instrumental resolution function,⁶² $f(Q)$ is the magnetic form factor⁶⁷ for Cu^{2+} , and g is the average g -factor, which is $g=2.083$ for CuHpCl.³⁸ Carrying out the integration of Eq. (2) for the band of intensity in Fig. 4(a) yields 0.7(1). The proximity of the value to $S(S+1)=3/4$ indicates that this band accounts for most of the magnetic scattering from CuHpCl. For a powder sample, the first moment $\hbar\langle\tilde{\omega}\rangle_Q$ of the measured quantity $\tilde{I}_m(Q,\hbar\omega)$ is related to the spherical average of Eq. (4), and is given by

$$\begin{aligned} \hbar\langle\tilde{\omega}\rangle_{\mathbf{Q}} &\equiv \hbar^2 \int_{-\infty}^{\infty} \omega \tilde{I}_m(\mathbf{Q}, \hbar\omega) d\omega \\ &= -\frac{2}{3} \left| \frac{g}{2} f(Q) \right|^2 \frac{1}{N} \sum_{\mathbf{r}, \mathbf{d}} J_{\mathbf{d}} \langle \mathbf{S}_{\mathbf{r}} \cdot \mathbf{S}_{\mathbf{r}+\mathbf{d}} \rangle \left(1 - \frac{\sin Qd}{Qd} \right), \end{aligned} \quad (7)$$

where $d=|\mathbf{d}|$. The first moment $\hbar\langle\tilde{\omega}\rangle_{\mathbf{Q}}$ computed from the data in Fig. 4(a) is shown in Fig. 15. In strongly dimerized systems, the term arising from the intra-dimer bond dominates the first moment.⁸ In the strongly dimerized two-leg ladder model of CuHpCl, these are the intramolecular rung bonds labeled by 1 in Table I and depicted in Fig. 3(a).³⁸ As shown by the dashed line in Fig. 15, the Q-dependence arising from inserting d_1 in Eq. 7 is manifestly inconsistent with the data. Specifically, the $d_1=3.376 \text{ \AA}$ bond yields a maximum at higher Q than is observed in the experiment. Thus a longer bond (or bonds) must give the dominant contribution to $\hbar\langle\tilde{\omega}\rangle_{\mathbf{Q}}$. Fitting the data in Fig. 15 to Eq. (7) with a single, variable bond length d_{α} yields $d_{\alpha}=7.5(2) \text{ \AA}$, and the dashed-dotted line shown in Fig. 15. However, this model is still inconsistent with the data. The salient discrepancy is that the ratio of the low-Q peak intensity to that of the high-Q plateau is about twice larger in the data than in the model. Such a large ratio can only be achieved by combining terms of varying sign in Eq. (7). With appropriate spin spacings, d , such terms can interfere destructively in the high-Q plateau while the low-Q regime is dominated by contributions from long bonds. Indeed, the solid line in Fig. 15, which we shall describe in greater detail below, corresponds to a model with both positive and negative terms in Eq. (7). According to this equation, the magnitude of the high-Q plateau is directly proportional to the shift of the ground state energy below zero, while the peak height measures the strength of individual spin pair contributions to the ground state energy. Hence, there is a direct link between a large peak to plateau ratio in first moment data, and frustrated interactions that raise the ground state energy.

The single-crystal data help to distinguish between the eight distinct spin pairs with Cu–Cu spacings in the range 7–7.6 Å. The first moment $\hbar\langle\tilde{\omega}\rangle_{\mathbf{Q}}$ of the magnetic scattering intensity, $\tilde{I}_m(\mathbf{Q}, \hbar\omega)$, from a single-crystalline sample is given by

$$\begin{aligned} \hbar\langle\tilde{\omega}\rangle_{\mathbf{Q}} &\equiv \hbar^2 \int_{-\infty}^{\infty} \omega \tilde{I}_m(\mathbf{Q}, \hbar\omega) d\omega \\ &= -\frac{2}{3} \left| \frac{g}{2} f(Q) \right|^2 \frac{1}{N} \sum_{\mathbf{r}, \mathbf{d}} J_{\mathbf{d}} \langle \mathbf{S}_{\mathbf{r}} \cdot \mathbf{S}_{\mathbf{r}+\mathbf{d}} \rangle (1 - \cos \mathbf{Q} \cdot \mathbf{d}). \end{aligned} \quad (8)$$

Here we have neglected any spin space anisotropy, a reasonable assumption for a spin-1/2 quantum spin liquid. The first moment may be determined from Gaussian fits to individual spectra as follows:

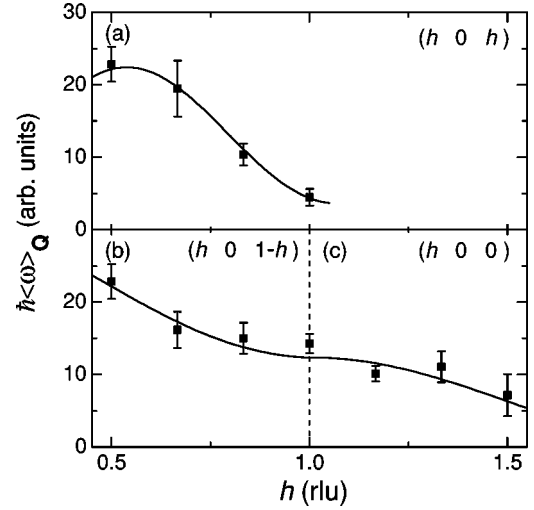


FIG. 16. First moment of the magnetic excitations in CuHpCl derived from single-crystal data. Curves are fits as described in text.

$$\hbar\langle\tilde{\omega}\rangle_{\mathbf{Q}} = \sum_i \tilde{I}_i(\mathbf{Q}) \hbar\omega_i(\mathbf{Q}), \quad (9)$$

where $\tilde{I}_i(\mathbf{Q})$ is the integrated intensity for mode i at wave vector \mathbf{Q} and $\hbar\omega_i(\mathbf{Q})$ is the corresponding mode energy. The wave vector dependence of $\hbar\langle\tilde{\omega}\rangle_{\mathbf{Q}}$ is illustrated in Fig. 6 where the diameter of the circles is proportional to $\hbar\langle\tilde{\omega}\rangle_{\mathbf{Q}}$ and as conventional plots along symmetry directions in Figs. 16 and 17. There is an undetermined overall scale factor as the single-crystal data were not normalized in this experiment. The first moment is seen to be largest for $h \approx 0.5$ along the line $(h01-h)$. Since the magnitude of \mathbf{Q} in that part of reciprocal space is close to the value 0.55 \AA^{-1} where the peak in the first moment of the powder data occurs, the powder and single-crystal data are consistent. The strongest modulation in $\hbar\langle\tilde{\omega}\rangle_{\mathbf{Q}}$ occurs along the $(h0h)$ direction, with

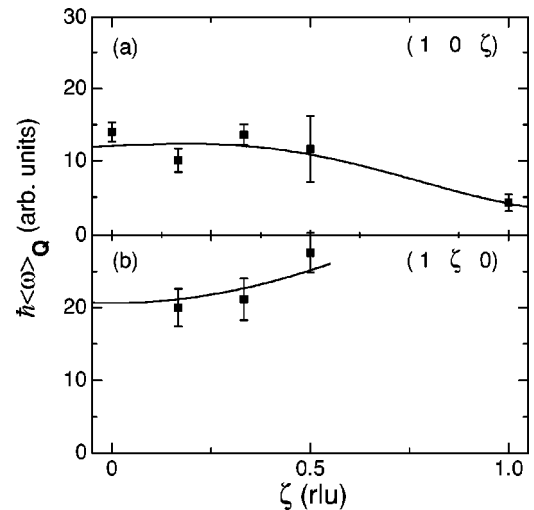


FIG. 17. First moment of the magnetic excitations in CuHpCl derived from single-crystal data. Curves are fits as described in text. Data from the $(hk0)$ zone were scaled to data from the $(h0l)$ zone using (100) as a point of reference.

weaker modulation also visible in other directions. From the form of Eq. (8), this implies that the bond vector that contributes most strongly to the first moment is parallel to $[101]$.

To determine the relative importance of the magnetic bonds, we carried out a simultaneous fit of the powder data to Eq. (7) and the single-crystal data to Eq. (8) with a single set of values for the bond energies, $J_a \langle \mathbf{S}_0 \cdot \mathbf{S}_a \rangle$. Because their contributions to the first moment of the scattering data cannot be distinguished, we derive only an average correlation term for spin pairs labeled with the same numerical index in Table I. Such spin pairs would be equivalent had the molecular unit possessed centro-symmetry. In addition, there is close similarity between the chemical environments along the exchange pathway of a and b labeled bonds. These facts lend some support to the assumption that the corresponding bond energies are similar.

The results of the fit are given in the last column of Table I and as solid lines in Figs. 15–17. It is important to note the direct contribution of a spin pair to the ground state energy is small when the exchange constant and/or the spin correlation function is small. Furthermore, according to Eq. (5), negative bond energies lower the ground state energy while positive terms indicate a frustrated spin pair that raises the ground state energy.

V. DISCUSSION

The most remarkable result from Table I, is that the intramolecular bond 1 is in a frustrated configuration. The presence of a frustrated spin pair with a short bond vector was anticipated based on inspection of the raw powder first moment data. It is easily verified that in a closed loop of interacting spins with an odd number of antiferromagnetic exchange interactions, only an even number of spin pairs can be satisfied. Bond 1 is part of no fewer than five near neighbor bond triangles that are frustrated if all interactions are antiferromagnetic. Figure 3(a) shows two of these triangles: (1,3,2) and (1,3,10). Figure 3(b) shows bond triangles (1,4,8) and (1,4,7), while Fig. 3(c) shows bond triangle (1,5,6). Of these, Table I clearly indicates that the triangles in Fig. 3(b) are frustrated. Our analysis indicates that bonds 4 and 8 are satisfied at the apparent expense of bond 1. The energy derived for bond 7 while negative, is not statistically significant. This is consistent with the expectation from Sec. I A that this is a weak exchange interaction.

The connectivity of the lattice formed by bonds 1, 4, and 8 is that of the geometrically frustrated Shastry-Sutherland model (SSM)³⁴ albeit with lower symmetry. Compared to the SSM, which can be described as a square lattice with alternating diagonal bonds on half the squares, the lattice shown by solid lines in Fig. 3(b) corresponds to a tetragonal lattice formed by bonds 4 and 8 with the “diagonal” bonds 1 arranged as in the SSM. When the square lattice exchange interactions in the SSM are less than 70% of the interactions across the diagonal, the ground state of the SSM consists of singlets on every cross bond.⁶⁸ For stronger inter-dimer interactions, there is a first order transition to square lattice Néel order. Table I indicates that the SSM planes in CuHpCl have local spin correlations resembling the Néel phase of the

SSM. The lattice formed by bonds 1, 5, and 6 also has the topology of the SSM but correlations in this plane do not readily map on a known phase of the SSM.

It does seem surprising that spin pair 1 can provide a three times larger positive contribution to the ground state energy than the negative contributions from bonds 4 and 8. To determine whether this is plausible, we examined a series of frustrated antiferromagnetic spin-1/2 clusters. A central spin pair, $\mathbf{S}_a, \mathbf{S}_b$ with antiferromagnetic exchange constant $J > 0$ is surrounded by $2n$ spins-1/2 $\mathbf{S}_1, \mathbf{S}_2, \dots, \mathbf{S}_{2n}$, which interact with both pair members with equal antiferromagnetic exchange, $J' > 0$. The spin Hamiltonian is given by

$$\mathcal{H} = \mathcal{H}_0 + \mathcal{H}_{2n}, \quad (10)$$

$$\mathcal{H}_0 = J \mathbf{S}_a \cdot \mathbf{S}_b, \quad (11)$$

$$\mathcal{H}_{2n} = J' \sum_{i=1}^{2n} \mathbf{S}_i \cdot (\mathbf{S}_a + \mathbf{S}_b). \quad (12)$$

We examined clusters with n ranging from 1 to 3. For each cluster we diagonalized the spin Hamiltonian and determined the ground state frustration index

$$f = -4n \frac{\langle 0 | \mathcal{H}_0 | 0 \rangle}{\langle 0 | \mathcal{H}_{2n} | 0 \rangle} \quad (13)$$

as a function of $x = J'/J$ in the range where the central spin pair is frustrated. We obtained maximum frustration indexes $f_{\max} = 1, 2, 3$ for $n = 1, 2, 3$, respectively. The results show that a level of frustration similar to that observed for the intramolecular spin pair in CuHpCl is possible even for very small spin clusters.

While the lattice of Fig. 3(b) provides an explanation for the frustration of bond 1, it does not readily account for the singlet ground state of CuHpCl. Local correlations in these planes is Néel-like so the lattice left on its own might be expected to have a gapless spectrum and long range order at low temperatures. From Table I we see that bond 3, which generates the lattice in Fig. 3(a), is in an unfrustrated configuration. In fact, this bond provides the greatest contribution towards lowering the ground state energy. Figure 14 shows how the lattices of Figs. 3(a)–3(c) intersect to form a three-dimensional lattice. We see that if the lattice in Fig. 3(b) were in a Néel phase, then bond 3 only serves to strengthen such Néel order and extend it to three dimensions. It is therefore difficult to see how the sub-lattices from Figs. 3(a) and 3(b) alone can account for an isolated singlet ground state.

This leads us to the suggestion that bonds 5 and 6 could play a significant role even if the corresponding bond energies appear to be small. As is apparent from Fig. 14, bonds 5 and 6 close a molecular triangle that projects onto the \mathbf{a}^* plane. The description therefore emerges of a set of antiferromagnetic SSM layers normal to \mathbf{a}^* coupled in a frustrating triangular lattice geometry to a second interpenetrating set of frustrated SSM layers normal to \mathbf{b}^* . A small alternation be-

tween the 3a and 3b bonds that couple layers could be an additional factor favoring singlet formation on the stronger of these bonds.

The magnetic ground state energy may be calculated from Eq. (5) and the numbers in Table I to be -0.36 meV per spin. For comparison, if all bonds were satisfied with the same magnitude of spin correlations as observed the ground state energy would be -1.17 meV per spin. The ratio between the actual ground state energy and the latter upper bound on the energy in the absence of frustration is 0.3. For comparison the ground state energy of the SSM at the critical point separating the Néel phase and the dimer phase is 0.26 times the energy that the spin system would have if all bonds could simultaneously be engaged in singlet formation.⁶⁹ Hence, CuHpCl is at least as frustrated as the SSM at its critical point.

VI. CONCLUSIONS

In summary, we have presented inelastic neutron scattering data from deuterated powder and hydrogenous single crystals of the organometallic spin-1/2 magnet CuHpCl. Consideration of the excitation spectra, the crystal structure, and the wave vector dependence of the first moment leads to the conclusion that spin-spin interactions in this system form a complex three-dimensional lattice and not a spin ladder as previously thought. While structurally one might expect CuHpCl to fall in the spin-dimer class of quantum spin liquids, this appears not to be the case. The spin gap in spin-dimer systems is a consequence of the singlet ground state of individual dimers. However, in CuHpCl the intra molecular spin interaction is in a frustrated configuration so this cannot be the dominant interaction in the problem. Furthermore, if the intra-molecular interaction is antiferromagnetic, as expected, then the ground state features triplet molecules that in and of themselves cannot explain a gap in the excitation spectrum. We are therefore led to the conclusion that the pronounced gap in the excitation spectrum of CuHpCl is a

consequence of the frustration inherent to this particular three-dimensional network of interactions. This is a surprising discovery as the symmetry of the lattice is low. On the other hand, the structure clearly is riddled with triangular units, and the connectivity between them is relatively low. These ingredients are known to be important for suppressing Néel order and promoting a spin liquid state.²² Further progress in understanding the magnetism of CuHpCl would benefit from accurate determination of H/D positions using neutron scattering, followed by quantum chemical calculations of exchange constants. More extensive measurements of the magnetic excitation spectrum are also needed, but these must await progress in crystal growth or neutron scattering instrumentation.

There are many organometallic quantum magnets that have been labeled as quasi-one-dimensional, based largely on the observation of a spin gap. Our experiments on CuHpCl have shown how neutron scattering from single crystals as small as 0.1 g can be used to establish the dimensionality and the basic nature of interacting spin systems. They also show that insulating magnets with a gap in their excitation spectrum may constitute a considerably more complex and diverse class of interacting quantum many-body systems than previously anticipated.

ACKNOWLEDGMENTS

We thank R. Paul for help with neutron activation analysis. This work was supported by NSF Grants Nos. DMR-9801742 and DMR-0074571. D.H.R. acknowledges the support of the David and Lucile Packard Foundation. T.L. acknowledges the support of the Sloan and Dreyfus Foundations. X-ray characterization was carried out using facilities maintained by the JHU MRSEC under NSF Grant No. DMR-0080031. This work utilized neutron research facilities supported by NIST and the NSF under Agreement No. DMR-9986442.

¹J. S. Miller and A. J. Epstein, *Mat. Chem. Adv. Chem. Series* **245**, 161 (1995); *Coord. Chem. Rev.* **206**, 651 (2000).

²*Dynamical Properties of Unconventional Magnetic Systems*, edited by A. T. Skjeltorp and D. Sherrington, NATO ASI Series, Series E: Applied Sciences, Vol. 349 (Kluwer Academic, Boston, 1998).

³K. Asano, Y. Miyazaki, W. Mori, K. Nakatani, O. Kahn, and M. Sorai, *Bull. Chem. Soc. Jpn.* **73**, 885 (2000).

⁴L. J. de Jongh and A. R. Miedema, *Adv. Phys.* **23**, 1 (1974); R. L. Carlin and L. J. De Jongh, *Chem. Rev.* **86**, 4 (1986).

⁵C. Broholm, D. H. Reich, G. Aeppli, S.-H. Lee, D. Dender, P. Hammar, Guangyong Xu, J. F. DiTusa, and A. P. Ramirez, in *Dynamical Properties of Unconventional Magnetic Systems*, edited by A. T. Skjeltorp and D. Sherrington, NATO ASI Series, Series E: Applied Sciences, Vol. 349 (Kluwer Academic, Boston, 1998), pp. 77–105.

⁶L. P. Regnault, J. Rossat-Mignod, J. P. Renard, M. Verdagner, and C. Vettier, *Physica B* **156-157**, 247 (1989), and refer-

ences therein; S. Ma, C. Broholm, D.H. Reich, B.J. Sternlieb, and R.W. Erwin, *Phys. Rev. Lett.* **69**, 3571 (1992).

⁷A. Zheludev, Y. Chen, C. L. Broholm, Z. Honda, and K. Katsumata, *Phys. Rev. B* **63**, 104410 (2001).

⁸G. Xu, C. Broholm, D. H. Reich, and M. A. Adams, *Phys. Rev. Lett.* **84**, 4465 (2000).

⁹D. C. Johnston, J. W. Johnson, D. P. Goshorn, and A. J. Jacobson, *Phys. Rev. B* **35**, 219 (1987).

¹⁰R. S. Eccleston, T. Barnes, J. Brody, and J. W. Johnson, *Phys. Rev. Lett.* **73**, 2626 (1994).

¹¹A. W. Garrett, S. E. Nagler, T. Barnes, and B. C. Sales, *Phys. Rev. B* **55**, 3631 (1997).

¹²A. W. Garrett, S. E. Nagler, D. A. Tennant, B. C. Sales, and T. Barnes, *Phys. Rev. Lett.* **79**, 745 (1997).

¹³S. A. Carter, B. Batlogg, R. J. Cava, J.J. Krajewski, W. F. Peck, Jr., and T. M. Rice, *Phys. Rev. Lett.* **77**, 1378 (1996).

¹⁴R. S. Eccleston, M. Uehara, J. Akimitsu, H. Eisaki, N. Motoyama,

- and S. Uchida, Phys. Rev. Lett. **81**, 1702 (1998).
- ¹⁵M. Matsuda, T. Yoshihama, K. Kakurai, and G. Shirane, Phys. Rev. B **59**, 1060 (1999).
 - ¹⁶B. C. Watson, V. N. Kotov, M. W. Meisel, D. W. Hall, G. E. Granroth, W. T. Montfrooij, S. E. Nagler, D. A. Jensen, R. Backov, M. A. Petruska, G. E. Fanucci, and D. R. Talham, Phys. Rev. Lett. **86**, 5168 (2001).
 - ¹⁷N. D. Mermin and H. Wagner, Phys. Rev. Lett. **17**, 1133 (1966).
 - ¹⁸B. Leuenberger, A. Stebler, H. U. Güdel, A. Furrer, R. Feile, and J. K. Kjems, Phys. Rev. B **30**, 6300 (1984).
 - ¹⁹Y. Sasago, K. Uchinokura, A. Zheludev, and G. Shirane, Phys. Rev. B **55**, 8357 (1997).
 - ²⁰N. Cavadini, W. Henggeler, A. Furrer, H. U. Güdel, K. Krämer, and H. Mutka, Eur. Phys. J. B **7**, 519 (1999).
 - ²¹N. Cavadini, G. Heigold, W. Henggeler, A. Furrer, H.-U. Güdel, K. Krämer, and H. Mutka, J. Phys.: Condens. Matter **12**, 5463 (2000).
 - ²²A. P. Ramirez, Annu. Rev. Mater. Sci. **24**, 453 (1994); Czech. J. Phys. **46**, 3247 Suppl. 6 (1996).
 - ²³P. W. Anderson, Phys. Rev. **102**, 1008 (1956).
 - ²⁴B. Canals and C. Lacroix, Phys. Rev. Lett. **80**, 2933 (1998).
 - ²⁵S. E. Palmer and J. T. Chalker, Phys. Rev. B **64**, 094412 (2001).
 - ²⁶R. Moessner and J.T. Chalker, Phys. Rev. Lett. **80**, 2929 (1998); Phys. Rev. B **57**, R5587 (1998); **58**, 12 049 (1998).
 - ²⁷S. H. Lee, C. Broholm, G. Aeppli, A. P. Ramirez, T. G. Perring, C. Carlile, M. Adams, and B. Hessen, Europhys. Lett. **35**, 127 (1996).
 - ²⁸I. S. Hagemann, Q. Huang, X. P. A. Gao, A. P. Ramirez, and R. J. Cava, Phys. Rev. Lett. **86**, 894 (2001).
 - ²⁹S.-H. Lee, C. Broholm, T.H. Kim, W. Ratcliff II, and S-W. Cheong, Phys. Rev. Lett. **84**, 3718 (2000).
 - ³⁰J. S. Gardner, B.D. Gaulin, S.-H. Lee, C. Broholm, N. P. Raju, and J. E. Greedan, Phys. Rev. Lett. **83**, 211 (1999).
 - ³¹S. Taniguchi, Y. Nishikawa, Y. Yasui, Y. Kobayashi, M. Sato, T. Nishioka, M. Kontani, and K. Sano, J. Phys. Soc. Jpn. **64**, 2758 (1995).
 - ³²H. Kageyama, K. Yoshimura, R. Stern, N. V. Mushnikov, K. Onizuka, M. Kato, K. Kosuge, C. P. Slichter, T. Goto, and Y. Ueda, Phys. Rev. Lett. **82**, 3168 (1999).
 - ³³M. B. Stone, I. A. Zalitznyak, Daniel H. Reich, and C. Broholm, Phys. Rev. B **64**, 144405 (2001).
 - ³⁴B. S. Shastry and B. Sutherland, Physica (Amsterdam) **108B**, 1069 (1981).
 - ³⁵H. Kageyama, M. Nishi, N. Aso, K. Onizuka, T. Yoshihama, K. Nukui, K. Kodama, K. Kakurai, and Y. Ueda, Phys. Rev. Lett. **84**, 5876 (2000).
 - ³⁶B. Chiari, O. Piovesana, T. Tarantelli, and P. F. Zanazzi, Inorg. Chem. **29**, 1172 (1990).
 - ³⁷P. R. Hammar and D. H. Reich, J. Appl. Phys. **79**, 5392 (1996).
 - ³⁸G. Chaboussant, P. A. Crowell, L. P. Lévy, O. Piovesana, A. Madouri, D. Mailly, Phys. Rev. B **55**, 3046 (1997).
 - ³⁹G. Chaboussant, M.-H. Julien, Y. Fagot-Revurat, L. P. Lévy, C. Berthier, M. Horvatić, and O. Piovesana, Phys. Rev. Lett. **79**, 925 (1997).
 - ⁴⁰G. Chaboussant, Y. Fagot-Revurat, M.-H. Julien, M. E. Hanson, C. Berthier, M. Horvatić, L. P. Lévy, and O. Piovesana, Phys. Rev. Lett. **80**, 2713 (1998).
 - ⁴¹P. R. Hammar, D. H. Reich, C. Broholm, and F. Trouw, Phys. Rev. B **57**, 7846 (1998).
 - ⁴²G. Chaboussant, M.-H. Julien, Y. Fagot-Revurat, M. Hanson, L. P. Lévy, C. Berthier, M. Horvatić, and O. Piovesana, Eur. Phys. J. B **6**, 167 (1998).
 - ⁴³M. Chiba, T. Fukui, Y. Ajiro, M. Hagiwara, T. Goto, and T. Kubo, Physica B **246-247**, 576 (1998).
 - ⁴⁴M. Hagiwara, Y. Narumi, K. Kindo, T. Nishida, M. Kaburagi, and T. Tonegawa, Physica B **246-247**, 234 (1998).
 - ⁴⁵H. Deguchi, S. Sumoto, S. Takagi, M. Mito, T. Kawae, K. Takeda, H. Nojiri, T. Sakon, and M. Motokawa, J. Phys. Soc. Jpn. **67**, 3707 (1998).
 - ⁴⁶R. Calemczuk, J. Riera, D. Píolblanc, J.-P. Boucher, G. Chaboussant, L. P. Lévy, and O. Piovesana, Eur. Phys. J. B **7**, 171 (1999).
 - ⁴⁷H. Ohta, T. Tanaka, S. Okubo, S. Kimura, H. Kikuchi, and H. Nagasawa, J. Phys. Soc. Jpn. **68**, 732 (1999).
 - ⁴⁸G. Chaboussant, M.-H. Julien, Y. Fagot-Revurat, M. Mayaffre, M. Horvatić, L. P. Lévy, C. Berthier, and O. Piovesana, Physica B **280**, 315 (2000).
 - ⁴⁹H. Mayaffre, M. Horvatić, C. Berthier, M.-H. Julien, P. Ségansan, L. Lévy, and O. Piovesana, Phys. Rev. Lett. **85**, 4795 (2000).
 - ⁵⁰N. Elstner and R. R. P. Singh, Phys. Rev. B **58**, 11 484 (1998).
 - ⁵¹T. Giamarchi and A. M. Tsvelik, Phys. Rev. B **59**, 11 398 (1999).
 - ⁵²X. Wang and L. Yu, Phys. Rev. Lett. **84**, 5399 (2000).
 - ⁵³B. Normand, J. Kyriakidis, and D. Loss, Ann. Phys. (Leipzig) **9**, 133 (2000).
 - ⁵⁴C. A. Hayward, D. Poilblanc, and L. P. Lévy, Phys. Rev. B **54**, R12649 (1996).
 - ⁵⁵M. Usami and S. Suga, Phys. Rev. B **58**, 14 401 (1998).
 - ⁵⁶Q. Gu and J. Shen, Phys. Lett. A **251**, 150 (1999).
 - ⁵⁷Q. Gu, D. Yu, J. Shen, Phys. Rev. B **60**, 3009 (1999).
 - ⁵⁸Z. Weihong, R. R. P. Singh, and J. Oitmaa, Phys. Rev. B **55**, 8052 (1997).
 - ⁵⁹M. Rodriguez, A. Llobet, and M. Corbella, Polyhedron **19**, 2483 (2000).
 - ⁶⁰Y. Yamada, N. Ueyama, T. Okamura, W. Mori, and A. Nakamura, Inorg. Chim. Acta **276**, 43 (1998), and references therein.
 - ⁶¹S. Kono and H. Watanabe, Chem. Abstr. **70**, 57917d (1969).
 - ⁶²N. D. Chesser and J. D. Axe, Acta Crystallogr., Sect. A: Cryst. Phys., Diffr., Theor. Gen. Crystallogr. **29**, 160 (1973).
 - ⁶³A. Furrer and H. U. Güdel, J. Magn. Magn. Mater. **14**, 256 (1979).
 - ⁶⁴K. Totsuka, S. Miyahara, and K. Ueda, Phys. Rev. Lett. **86**, 520 (2001).
 - ⁶⁵S.W. Lovesey, *Theory of Neutron Scattering from Condensed Matter* (Clarendon, Oxford, 1984).
 - ⁶⁶P. C. Hohenberg and W. F. Brinkman, Phys. Rev. B **10**, 128 (1974).
 - ⁶⁷P. J. Brown, in *International Tables for Crystallography*, edited by A. J. C. Wilson, Vol. C (Kluwer Academic, London, 1995).
 - ⁶⁸E. Müller-Hartmann, R. R. P. Singh, C. Knetter, and Götz S. Uhrig, Phys. Rev. Lett. **84**, 1808 (2000).
 - ⁶⁹Y. Takushima, A. Koga, and N. Kawakami, J. Phys. Soc. Jpn. **70**, 1369 (2001).